Triply periodic minimal surface based lattices for acoustic performance

CHOUHAN, Ganesh, BIDARE, Prveen and BALA MURALI, Gunji

Triply Periodic Minimal Surface Based Lattices for Acoustic Performance

Ganesh Chouhan[1*], Prveen Bidare[2],Gunji BalaMurali[1]

[1]*School of Mechanical Engineering, Vellore Institute of Technology, Vellore 632014 Tamil Nadu, India.*

[2]*Department of Engineering and Mathematics, Sheffield Hallam University, Howard St, Sheffield City Centre, Sheffield S1 1WB, U.K*

Abstract

Environmental noise pollution is exacerbated by accelerated urbanization and different sources generate a unique sound spectrum. To address the aforementioned issue, triply periodic minimal surface acoustic absorbers were additively manufactured with three geometrical parameters (porosity, sample thickness, and wall thickness) patterns to absorb sound across a wide range of frequencies. TPMS absorbers made from Abs resin were manufactured using VAT polymerization additive manufacturing (SLA) technology. The acoustic properties of these absorbers were evaluated using the impedance tube technique across a frequency range of 100-6400Hz and discussed. The four TPMS absorbers exhibit slight variations in density as a result of their distinct unit cell sizes, which are necessary to uphold constant porosity levels. This study found multiple parameters, especially the nature of the surfaces, porosity ranges, sample thicknesses, and wall thickness of the tested sound-absorbing TPMS 3D printed structure, significantly impacted the sound absorption performance. At the ideal process parameters of 80% lattice porosity, 60mm sample thickness, and 0.8mm wall thickness, the gyroid lattice obtained a peak sound absorption coefficient of 0.945, a noise reduction coefficient of 0.50, and an average sound absorption of 0.575. The suggested 3D-printed TPMS acoustic absorbers, inspired by nature, can be placed on construction walls or transportation applications, depending on the desired acoustic absorption range.

***Keywords*:** Lattice structure, Triply periodic minimal surface, Additive manufacturing, Sound absorption, Noise reduction coefficient.

1. Introduction

TPMS lattices are among the most significant structures that exhibit exceptional mechanical strength [1], improved heat transfer efficiency [2], and superior sound absorption performance [3]. These designs optimize the acoustic characteristics at both low and high frequencies while minimizing the material usage. Diesel generators in society or chiller rooms in industries, known for their excessive noise output, require a robust and compact wall or cabin that effectively absorbs a substantial quantity of sound and maintains the minimum airflow. Additive manufacturing of triply periodic minimum surface lattices has recently attracted considerable interest owing to its role in several challenging situations, including aerospace, automobile, and biomedical industries [4–6]. However, due to their intricate layout, TPMS-based lattices can only be produced via additive manufacturing techniques [7].

1.1. Lattice structures; applications and engineering models

Lattice structures are three-dimensional structures composed of linked units ordered in a repeating pattern [8], such as triply periodic minimal surfaces and strut-based structures [9] (see **Figure 1)**. Owing to their remarkable properties, lattice structures are often employed in the development of modern engineering structures. Sound absorption and reflection are used in traditional materials and designs to restrict sound transmission across a boundary. However, these structures often impede both acoustic wave propagation and continuous fluid flow across the boundary. This feature severely restricts their use in cases where air movement is required or advantageous, such as noise reduction in locations where ventilation necessitates that air flows freely. Lattices are trending due to their complex shapes [10], lightweight [11], consuming less material, and providing a larger surface area with a higher thermal rate [12], mechanical strength [13], and sound resistance [14]. The size and shape of a lattice structure might be homogeneous or non-homogeneous. In a few scientific studies, cellular and lattices have minor differences, Although lattice structures offer superior performance to foams and honeycombs [15].

1.2. TPMS-based lattice structures, design, and characterization

Complex geometries offer broad curved areas that permit sound waves to penetrate within, which are essential for achieving better sound absorption performance. Jiaming Bai [16], and Chen H [17] defined “TPMS is a non-intersecting 3D surface with a mean curvature of zero at each point.” These structures are the complex implicit surface and are adopted in

mass-customized implants for bio-engineering [18], functionally graded structural [19], heat transfer equipment such as heat exchangers [20] and heat sinks [2], catalytic substrates [21], robotic arms [22], feed spacers [23], and bioreactor media for wastewater treatment [24] are just a few success stories.

Chunguan Lin et al. [25] performed the parametric study of two TPMS-based sandwich panels (P and G surfaces) and the panels were made with a high-resolution SLA 3D printer with a bonding method. The performance of sandwich panels as sound insulators has been studied theoretically using Reissner's theory and numerically using COMSOL Multiphysics (pressure acoustics and solid mechanics coupled). It has been found that G-type TPMS sandwich panels performed impressively, especially at low frequencies, and had prominent mechanical propertie. The three polymethyl methacrylate-based TPMS lattices exhibited multiple band gaps between 200 and 2000 Hz in the frequency range [26]. The slow-sound lattice sound absorber used different truss-like structures and achieved an improved sound absorption coefficient in the frequency range from 1000 to 6300 Hz [27]. In a 3D-printed open porous lattice, material thickness, air gap, and excitation frequency all significantly affect airflow resistivity and, consequently, the effectiveness of sound absorption [28]. A metal 3D-printed sandwich lattice demonstrated outstanding sound insulation features over an entire frequency range [29].

1.3. Acoustic models and terminology

Kimura M. et al. [30] developed the high-frequency impedance tube apparatus using ASTM E1050/ISO10534-2 and ASTM E2611 guidelines. The tube can measure acoustic performance up to 12.8 kHz, and results have been validated with a conventional impedance tube and an open cavity condition. In their study, Yujun Zhao et al. [31] examined the acoustic characteristics of fibrous material through various methods, such as the inverse method based on the Johnson-Champoux-Allard equation, the two-thickness approach, the four-microphone transfer function matrix, and the finite transfer matrix. A mathematical model based on neural networks and particle swarm optimization (PSO) was presented to reduce the errors in the sound absorption coefficient results. The PSO model performed similarly to commercial Brüel & Kjær tubes at all frequency levels, with an error reduction of 37% [32].

The high noise level is above 85 dB, and over a prolonged period may start to damage normal ears [33]. As a result, several strategies have been created to keep noise levels within

the recommended ranges, one of which is the use of traditional noise reduction materials, mainly including sound-absorbing materials (fiber, glass, mineral wool, foam, and perforated plates), sound insulating materials (metal, inorganic, and polymer composites), and noise damping materials (viscoelastic, high damping-alloys and composites) [34].

The noise reduction coefficient (NRC) is an arithmetic mean of the sound absorption coefficients at frequencies of 250, 500, 1000, and 2000 Hz [35]. In essence, NRC is one value that indicates the ability of an acoustic material to absorb sound and operate from 0.0 to 1. Better sound absorption ability is indicated by higher NRC values; buildings with values above 0.5 are considered to be good absorbers. NRC values of 0 and unity denote complete reflection and absorption, respectively [36].

1.4. Additive manufacturing, technique to develop TPMS lattice

The lattices have intricate 3D geometry, and traditional production methods have encountered major challenges. Advances in additive manufacturing are assisting in addressing this manufacturing difficulty [37]. 3D printing currently provides for effective control of lattice geometry on a micrometer to a centimeter scale, and it is expanding at a higher pace than ever before [38, 39]. By layering materials onto a product and only depositing them where they are necessary, additive manufacturing, or AM, significantly reduces both the amount of material used and the amount of waste that is produced [40]. Among the few additive manufacturing families, stereolithography (SLA), fused filament fabrication (FFF), and digital light processing (DLP) have successfully produced thermoplastic [41], and thermosetting [42] lattice structures. In these processes, the material is cured using an energy source (laser) to build a 3D structure.

1.5. Scope and contribution of the study

In previous studies, many structures have been extensively studied for improving absorption performance at particular frequencies, including body-centered cubic, face-centered cubic [43], pyramidal [44], honeycomb [45], and metamaterials [46]. The adoption of additive manufacturing for developing TPMS-based (Primitive, Gyroid, and Diamond) sound absorbers for upper midrange frequency has been addressed by Yang et al. [3], The author selected three geometry parameters including volume fraction, unit cell size and height, and diamond lattice proven better results in wide bandwidth. Unlike volume-based lattices, TPMS structures are gaining more adoption in sound absorption applications. The

current work covers a broad range of porosities, lengths of samples, sample diameters, wall thicknesses, and extra lattice surfaces (lidinoid) to explore acoustic behaviors.

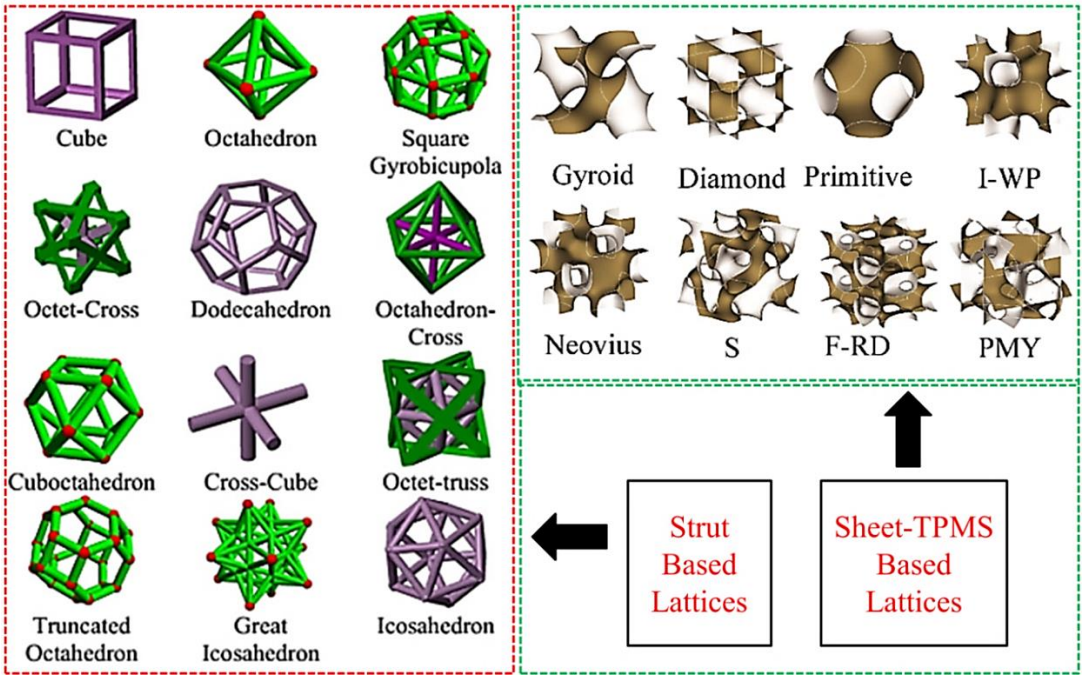

Figure 1 Different types of lattice structures [9].

In this work, we proposed four TPMS-based (Gyroid, split P, diamond, and lidinoid) lattices for sound absorption applications that block maximum sound while allowing or limiting airflow. The work was accomplished in four stages, including:

1. The design of four TPMS structures with four porosities with an explanation of their self-supporting behavior.
2. The development of techniques using stereolithography 3D printing, which covered pre and post-processing for samples.
3. Measurement of sound absorption and NRC of the printed lattice.
4. Study the effects of sample thickness and wall thickness.

Furthermore, the selected parameters directly affect the sound absorption at the targeted frequency and were analyzed for optimum absorption.

1.6. Outline of the Paper

The outline of the paper is as follows: Section 2 presents the tools utilized in this investigation. section 2.1 discusses the principles of sound absorption. section 2.2 presents the mathematical designs of all four TPMS specimens 2.3. section discusses the self-supportive behavior of lattices. The additive manufacturing approach for obtaining the

acoustic model parameters is summarized in section 2.4 together with a testing method. The study outcomes are given in Section 3, where Section 3.1 specifically covers the measurements of the sound absorption mechanism of TPMS Structures. Subsequently, the subsection discusses the impact of porosity, various surfaces, sample thickness, and wall thicknesses. The analysis of curve fitting is offered for all lattices in paragraph 3.1.2. A concise overview is provided in Section 4.

2. Method and Material

2.1. Principles of sound absorption

Sound absorption is the phenomenon that describes how sound waves lose power as they encounter a lattice structure. It involves three major types of transformations: reflection, absorption, and transmission. **Figure 2** demonstrates that the sum of the reflected, absorbed, and transmitted energy can be considered the total sound energy.

$$E_i = E_r + E_a + E_t \quad (1)$$

Where E_i is the total incident energy on the lattice structure, E_r is the reflection energy, E_a is an absorption energy, and E_t is the transmission energy.

The sound absorption coefficient (α) is the ratio of absorbed energy in material to incident energy, which can be experimentally tested by an impedance tube or reverberation chamber [47]. The following equation is employed to measure the sound absorption coefficient:

$$\alpha = \frac{E_a}{E_i} = 1 - \frac{E_r}{E_i} \quad (2)$$

In general, several variables affect the sound absorption property of a material, including the type of material, the excitation wave frequency, airflow resistivity, thickness, pore size, temperature, density, and humidity. The airflow resistivity helps predict the sound absorption coefficient of the material and is tested using the ISO 9053-1:2018(E) standard [48].

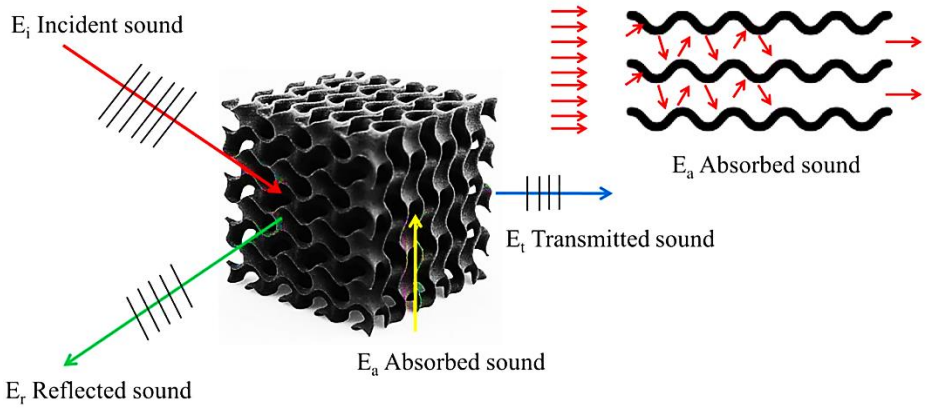

Figure 2 Sound absorption mechanism.

Sound absorption coefficients, specific impedances, and sound transmission losses of acoustic materials are often measured using two-microphone transfer function methods. This method has the benefit of obtaining both the sound absorption coefficient and surface impedance values in a single experiment. A signal generator uses a speaker to create a sound pressure wave, which is then delivered into the tube. This wave loses some of its energy as it strikes the fixed specimen at the other end of the tube, returning with a smaller amplitude. The incident wave (HI) and reflected wave (HR) of transfer functions are expressed as follows:

$$H_1 = \frac{P_{2l}}{P_{1l}} = e^{-jk\,(x_1 - x_2)} = e^{-jks} \tag{3}$$

$$H_R = \frac{P_{2R}}{P_{1R}} = e^{jk\,(x_1 - x_2)} = e^{jks} \tag{4}$$

k denotes wave number (air), s is the mice spacing between the microphones and the specimen as x1 and x2., and j is an imaginary component. P_{1l} and P_{1R} stand for incident wave and P_{2l} and P_{2R} reflected wave for microphones 1 and 2.

$$H_{12} = \frac{P_2}{P_1} = \frac{e^{jkx_2} + R\,(e^{-jkx_2})}{e^{jkx_1} + R\,(e^{-jkx_1})} \tag{5}$$

The reflection coefficient (R) can be obtained as follows:

$$\mathrm{R} = 1 - \left|\frac{Z_s - \rho_0 c_0}{Z_s + \rho_0 c_0}\right|^2 \tag{6}$$

The specific impedance ratio ($Z_s/\rho_0 c_0$), and the sound absorption coefficients (α) can be calculated from the reflection coefficient (R). Where Z_s presents surface impedance, while $\rho_0 c_0$ represents the impedance of air [49].

$$\alpha = 1 - |R|^2 = 1 - \left|\frac{Z_s - \rho_0 c_0}{Z_s + \rho_0 c_0}\right|^2 \quad (7)$$

As the arithmetic mean of the sound absorption coefficient for frequencies between 250 and 2000 Hz, NRC is one of the simplest methods to estimate.

$$\boldsymbol{NRC} = \frac{\alpha_{250} + \alpha_{500} + \alpha_{1000} + \alpha_{2000}}{4} \quad (8)$$

2.2. Design of the TPMS Lattice Absorbers

Within this contribution, generic lattice test samples are designed using a triply periodic minimal surface lattice design. The four TPMS structures- Gyroid, Split P, Lidinoid, and Diamond have been designed using level-set approximation equations to investigate sound absorption characteristics. The Fourier transformation created TPMS structures by deriving a 3-dimensional mathematical expression of f(x, y, z) = t, where 't' is a level-set constant for each geometry and t = 0 for sheet-based TPMS structures. The designs offer the most significant ratio of surface area to volume and are appropriate for applications such as heat transfer [50]. The approximation equations can help to develop the structures [51–53].

1. Diamond

$$f(X,Y,Z) = sinX\ sinY\ sinZ + sinX\ cosY\ cosZ + cosX\ cosY\ sinZ \quad (9)$$

2. Gyroid

$$f(X,Y,Z) = \sin X \cos Y + \sin Z \cos X + \sin Y \cos Z \quad (10)$$

3. Split P

$$f(X,Y,Z) = 1.1(\sin 2X \sin Z \cos Y + \sin 2Y \sin X \cos Z + \sin 2Z \sin Y \cos X) - 0.2(\cos 2X \cos 2Y + \cos 2Y \cos 2Z + \cos 2Z \cos 2X) - 0.4\ (\cos 2X + \cos 2Y + \cos 2Z) \quad (11)$$

4. Lidinoid

$$f(X,Y,Z) = \sin 2X \cos X\ \sin Z + \sin 2Y \cos Z \sin(X) + \sin 2Z \cos X \sin Y - \cos 2X \cos 2Y - \cos 2Y \cos 2Z - \cos 2Z \cos 2X + 0.3 \quad (12)$$

where $X = \omega x$, $Y = \omega y$, $Z = \omega z$ are the spatial coordinates and ω is the function periodicity given as

$$\omega = \frac{2\pi}{l}, \quad (13)$$

The porosity range of 80-92% was chosen because structures with porosity below 80% were denser, while those beyond 92% were highly porous. The sample height of 55-60-65mm was a progressive preference, involving the design of a lattice cabin wall to reduce external noise while maintaining high mechanical strength.

Prior to additive manufacturing, cylindrical computer-aided design (CAD) models were designed with nTopology software by repeatedly replicating unit cells. nTopology is implicit design software that enables designers and manufacturers to develop any shape, no matter

how complicated, and yet satisfy the demands of high-performance solutions. **Figure 3** depicts the basic design functions chosen for the gyroid lattice. First, hollow cylinders with a radius of 16 mm and a height of 60 mm were produced using the 'cylinder' function. Then, the walled TPMS function was used to draw a gyroid lattice with a particular cell size and wall thickness. The final design has been accomplished through the use of the boolean union command, which merges the cylinder and gyroid lattice. The wall thickness of lattices was kept at 1 mm. In order to find out the mass and volume of the design, the 'mass property function from the body' was utilized, which is crucial in calculating the porosity value.

Table 1 indicates that, while preserving a constant porosity, the unit cell sizes of each lattice are unique due to their varying degrees of complexity. The level of complexity can be observed for a constant 80% porosity lattices, where the lidinoid depicts the highest complexity and dense structure. The factor porosity directly impacts unit cell size and structure volume; as cell size increases, structure volume decreases. To maintain 80% porosity, the lidinoid design needed 19 mm unit cells, but the gyroid lattice needed just 9.75 mm. The volume of the four different structures in the four porosity ranges shows a slight difference.

Table 1 Parametric details of TPMS lattices and different complexity levels in lattices.

Structure Type	Volume Porosity(%)	Cell Size x/y/z(mm)	Structure Volume(mm^3)	Complexity in Lattices for 80% Porosity
Gyroid G	80 85 90 92	9.75 13 19.25 23.5	8470.8 6363.63 4280.3 3393.06	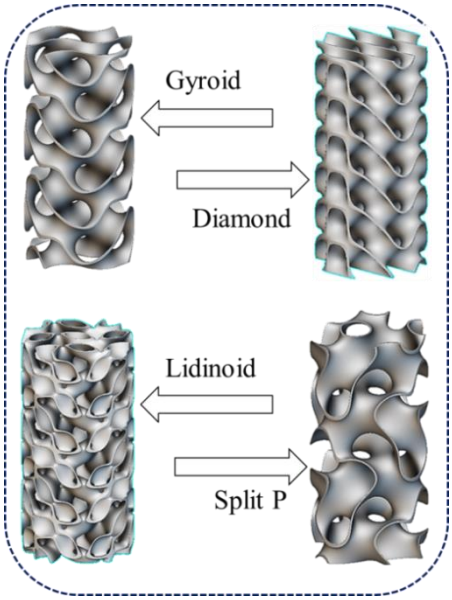
Diamond D	80 85 90 92	11.6 15.6 23.5 28.9	8509.6 6368.7 4139.2 3365.4	
Lidinoid L	80 85 90 92	19 25.1 38.2 46	8482.14 6340.6 4217.0 3370.0	
Split P P	80 85 90 92	12.8 17.6 26.55 34.5	8448.2 6333.4 4217.7 3374.7	

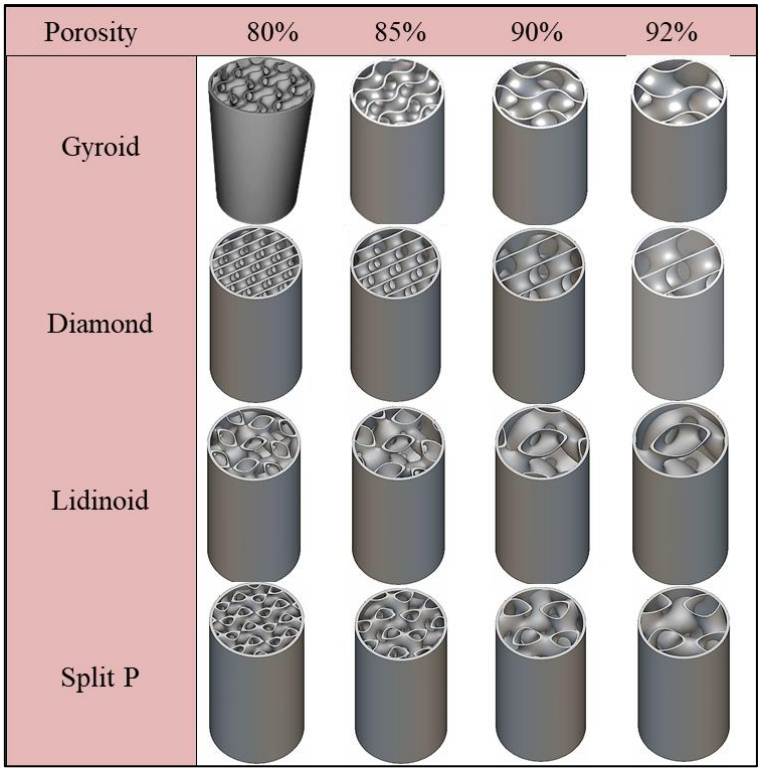

Figure 3 Design of TPMS lattice according to different porosity percentages.

2.3 Self-Supported Nature of TPMS Lattice

By employing 3D printing, intricate structures can be produced; however, hanging surfaces need support systems. It uses costly raw materials, takes a long time to manufacture, and requires considerable energy [54]. Similar to this, there is rising interest in creating more complex, lightweight cellular structures that can be manufactured in a variety of cell sizes and volume fractions and are self-supporting. Due to these restrictions, designers opted for triply periodic minimum surfaces (TPMS) architectures. The unique inner self-supporting structures are called triply periodic minimum surfaces. These structures may be altered to create complex structures for a variety of uses, including heat exchangers and tissue engineering. The self-supporting nature of these structures makes them suitable for use as infill patterns [55].

The triply periodic minimum surface structures are composed of a small slice of the surface that is assembled into the whole surface by translating repetitions of the basic piece in three distinct directions in the area. The slicing software Chitubox 1.8.1 has been used, and the layer's behavior at five different layers has been addressed for all samples. **Figure 4** reflects the self-supportive mechanisms of different TPMS-based structures. Each surface demonstrates the connections with other surfaces to support it and for each layer, the

structure pattern is changing. The surface behavior of all samples shows that TPMS structures are the ideal candidates to print without a support system during 3D printing. These structures are the best solution when it is necessary to print a structure in a shell or infill in any shape without the requirement of supports for hanging surfaces.

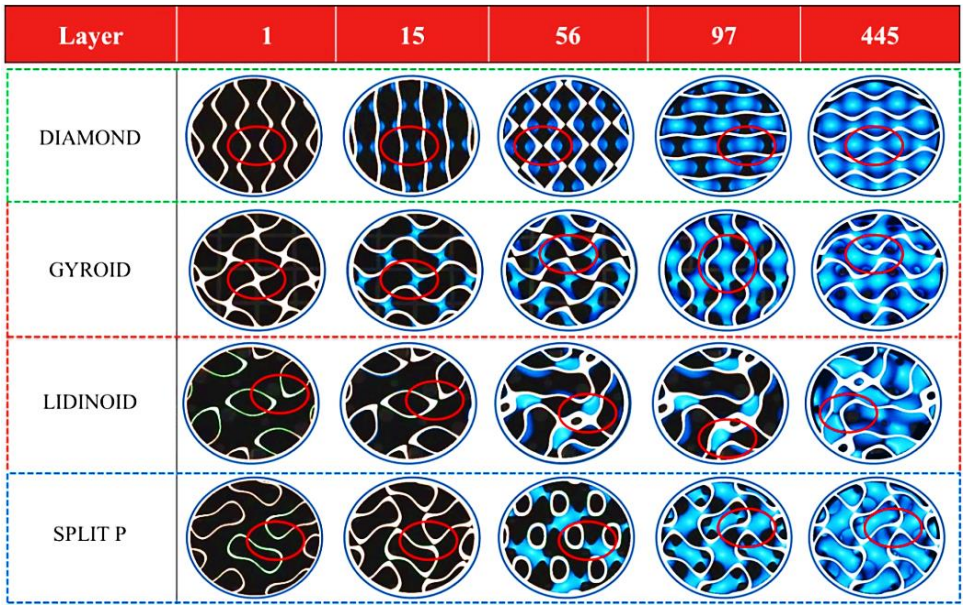

Figure 4 Self-supportive nature of TPMS structures.

2.4 Additive Manufacturing and Testing

Experimental samples have been manufactured using ELEGOO ABS standard photopolymer resin (405nm). ABS resin is one of the thermosetting polymers frequently employed in 3D printing. It is lightweight, abrasion-resistant, and heat-resistant [56] and is used for the fabrication of low-cost architectural models and prototypes for engineering. The test samples were manufactured using Creality LD002R LCD 3D stereolithography machine. The machine possesses the following functions:

- Build Volume: x = 119 mm; y = 65 mm; z = 160 mm
- XY axis resolution: 0.00185 inches / 0.047mm
- precision:0.075mm
- Print speed: 6-18 s/layer
- UV light source: 405nm wavelength
- Nominal power: 72W
- Slicing Software: Chitubox (CHUANGBIDE Technologies Co., Ltd.)

The CAD model has been saved in STL format and transferred to slicer software to convert the machine-readable format. The m/c also provides sample fabrication information such as the resin volume, mass of the part, and printing duration. For 3D-printed samples to have a high level of surface finish and strength, post-processing is a vital step [57]. Printing

three samples in a single pass sped up the printing process. The machine takes 4 hours, 44 minutes, and 43 seconds to print one component, and three pieces require the same period. All the parts were printed in a flat orientation and without support (TPMS structures are self-supportive). In subsequent stages of the printing procedure, the samples were immersed in a high-quality isopropyl alcohol solution for 15 minutes and then exposed to the curing process, i.e., a 405 nm UV laser. The procedure was carried out for around 30 minutes. **Figure 5(a)** presents the 16 printed samples of TPMS lattices for different porosities. The printing dimensions of all samples were confirmed by the use of vernier calipers and radius gauges. The print quality of all samples was remarkable and significantly superior to that of FDM 3D printing techniques. A total of 24 samples have been manufactured for testing

Experiments have been carried out to verify and highlight the effective absorption characteristics of the TPMS lattices presented. The experiments were conducted using a Holmarc ITC219 impedance tube system, as depicted in Figure 5(b). Reliable testing frequencies of 0.5 to 6.3 kHz were provided by impedance tube. In the sample holder, specimens were loaded at the impedance tube's end with a hard backing. Each stated absorption coefficient curve was the average of the results from at least three measurements. The ASTM E1050 standard norms were maintained during each examination, such as testing room temperature, barometric pressure, relative humidity, and sound speed (25°C, 101.325 Pa, 65%, 346.11 m/s). Both microphones and the system were calibrated to ensure accurate frequency response function readings. The testing results show a better sound absorption coefficient for all TPMS structures with lower porosity.

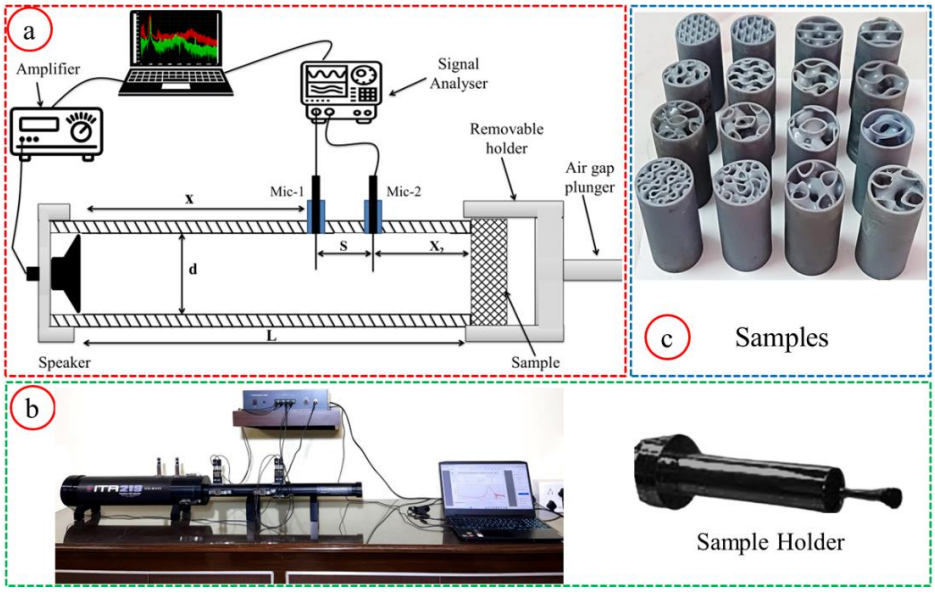

Figure 5 a) Terminology of impedance tube, b) Impedance tube testing setup, and c) Printed specimens.

3. Results and Discussion

The main objective of the presented study is to explore the acoustic response of 3D-printed TPMS-based structures. The results discussed the impact of surfaces, porosities, sample thickness, and wall thickness on acoustic absorption performance at various frequencies and concluded the most suitable TPMS-based structures in terms of sound absorption.

3.1 Sound Absorption Mechanism of TPMS Structures- Effect of the Porosity

The experimentally obtained sound absorption coefficient results of four TPMS lattice structures are presented in **Figure 6**. The comparison of the calculated responses of Gyroid, Diamond, Lidinoid, and Split P over the frequency range of 100 Hz to 6000 Hz has been discussed for the porosity range of 80%, 85%, 90%, and 92%. Apparently, it was found that at 92% porosity, the gyroid specimen responds slide differently to the diamond specimen, whereas the split P sample presents the smallest sound absorption value among the designs, as plotted in **Figure 6**. The highest absorption coefficient at 92% porosity was achieved for the gyroid lattice ($\alpha = 0.67$) with fixed height and diameter at the higher frequency ranges. The findings show that acoustic absorption decreases as porosity increases, yet the frequency range of maximum absorption grows. Moreover, higher porosity (90-92%) diamond lattices show an early peak of sound absorption than gyroid samples and opposite results were noticed for lower porosity (80-85%) samples.

The findings indicate that all lattice samples with 90% porosity have a higher overall absorption coefficient than those with 92% porosity same lattices, and it was more than 23%. In addition, The first peak absorption coefficient for 80-85-90% porosity gyroid samples was achieved at a frequency range of 1000-2000Hz. The absorption coefficient value was positively increased by an increase in porosity up to 90%. The mean value of the absorption coefficient for Gyroid and diamond is 0.68 and 0.70, which is much higher than split P and lidinoid values of 0.50 and 0.41, respectively, which means that in the same frequency range and at 90% porosity level, gyroid and diamond absorb sound about 35% better than split P and lidinoid. Similar to the 92% porosity results, gyroid and diamond lattices exceed the 32% average absorption of split P and lidinoid structures with the same frequency. The data shown above clearly show that, as porosity rises, density drops and pore size grows. The flow resistance decreases as the pore size and surface finish increase.

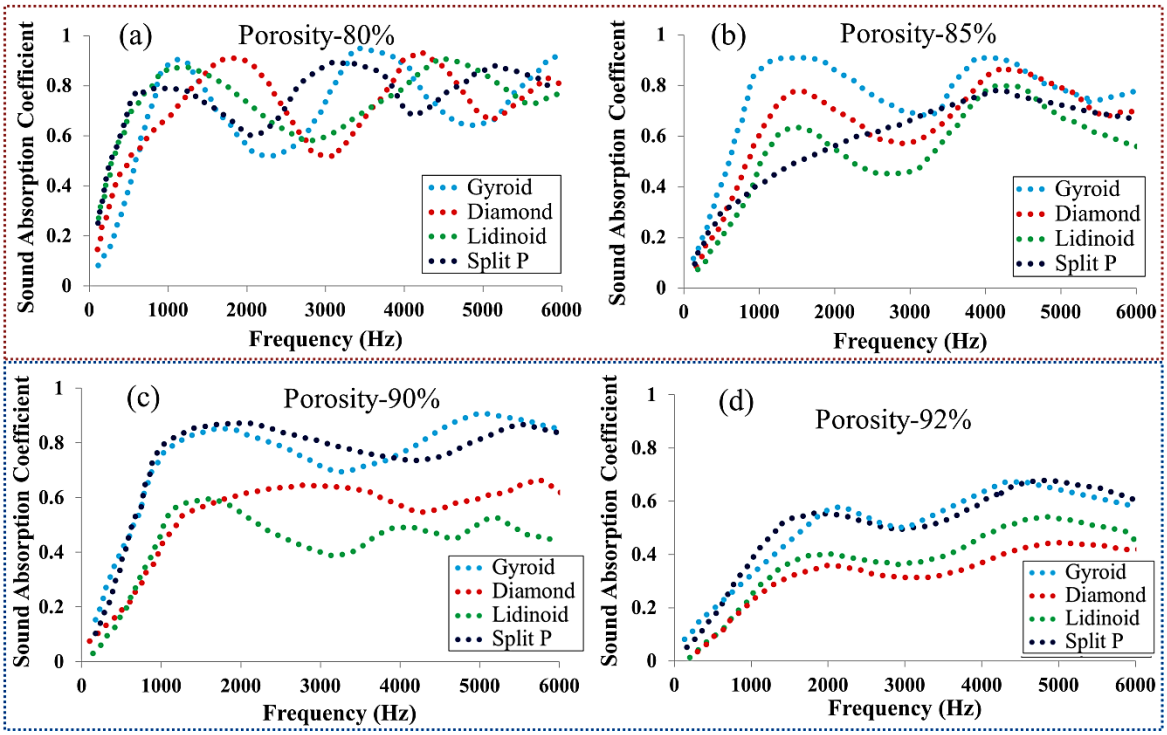

Figure 6 (a-d) Sound absorption results for 80-85-90 and 92% porosity TPMS structures.

A similar pattern has been observed in **Figure 6(a-b),** gyroid and diamond lattices revealing more significant absorption results in a lower porosity range. The highest sound absorption has been noted for gyroid lattice (0.945) in the 80% porosity range, while diamond achieved 0.936. For 80% porous Gyroid, Diamond, and Lidinoid samples, the sound absorption coefficient is more than 0.8 at a frequency of 725-1845 Hz. Again, the Split P has the lowest sound absorption rating. The initial peak absorption coefficients of the gyroid and diamond lattices occur at 1092 and 1786 Hz, respectively. The voids are smaller in lower porosity lattices, and the values of the absorption coefficient throughout the whole range of frequencies are larger than for higher porosity lattices. Gyroid has an absorption coefficient of 0.90 for the first maximum at 1092 Hz for 80% porosity, whereas gyroid with 90% porosity has an absorption coefficient of 0.86 for the first maximum at 1620 Hz.

At 85% porosity, the Gyroid, Diamond, and Lidinoid exhibited identical absorption behaviors, with two-peak resonance absorption coefficients ranging from 0.63 to 0.90 at around 1500 and 4500 Hz. At the initial resonance frequency, the optimum absorption results for the gyroid, diamond, and lidinoid lattices are 0.9104 (1561.80 Hz), 0.777 (1567.90 Hz), and 0.635 (1554.80 Hz), respectively, while 0.9109 (3968 Hz), 0.8735 (4233.2 Hz), and 0.7991 (4188.4 Hz) result for the second resonance frequency. The two-peak absorption results of gyroid lattice were marginally more significant than those of lattice diamond and lidinoid.

3.2 Curve fitting analysis

The purpose of the curve fitting is to identify the best lattice for specific applications in given frequency and porosity ranges. Four distinct TPMS lattices with different porosities have been displayed in Figure **7** to attempt the best effective curve fit between the experimental frequency and SAC data. The quadratic polynomial fitting method has been used in JMP Pro-17. A dotted line curve indicates the experimental fitting result and a solid line denotes the best curve fit. The curve fitting results for the diamond lattice with 92% porosity agree well with the experimental values over a wide frequency range (R^2: 0.828813), but the sample with 80% porosity gives the worst results (R^2: 0.31484). In comparison to the best-fit curve, a low-porosity diamond's average fitness value is substantially lower. The fitting curve shows average results for 85% and 90% diamond lattices. A 92% porosity gyroid lattice has been found to have the best curve fit; however, an 80% sample yields the lowest scores across all porosity ranges. The optimum agreement with experimental data is shown by the top three porosity split P lattices, and the most promising result is shown by the 85% porosity sample out of all the structures. In accordance with the best-fit curve, all structures in the porosity and solidity categories exhibit the following accuracy sequence for the R square value: 92%>85%>90%>80%. The lattices with 80% porosity had a greater deviation, but the split p lattice with 85% porosity and the gyroid lattice with 92% porosity demonstrated the lowest differences.

Structure	80%	85%	90%	92%
Diamond	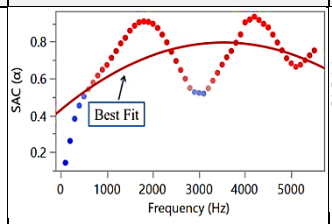	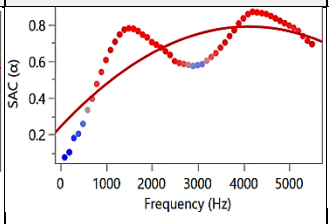	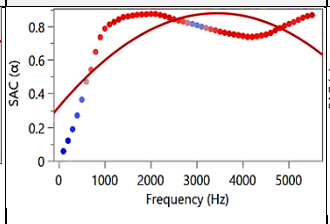	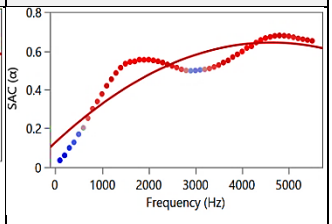
Polynomial Fit Degree=2	SAC = 0.6590315 + 4.2935e-5*Frequency - 2.9303e-8*(Frequency-2800)^2 **R^2: 0.31484**	SAC = 0.4916238 + 8.5136e-5*Frequency - 3.2169e-8*(Frequency-2800)^2 **R^2: 0.637559**	SAC = 0.6895021 + 5.996e-5*Frequency - 4.7194e-8*(Frequency-2800)^2 **R^2: 0.570386**	SAC = 0.3162606 + 8.7737e-5*Frequency - 2.4055e-8*(Frequency-2800)^2 **R^2: 0.828813**
Gyroid	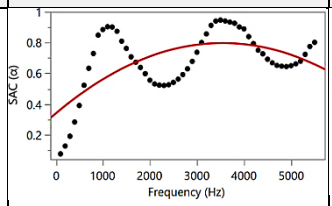	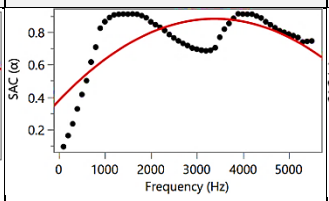	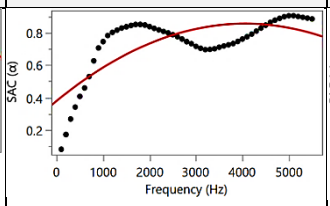	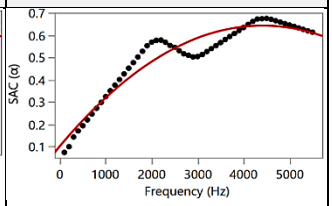
Polynomial Fit Degree=2	SAC = 0.6242663 + 5.4371e-5*Frequency - 3.6379e-8*(Frequency-2800)^2 **R^2: 0.35838**	SAC = 0.7207102 + 5.1475e-5*Frequency - 4.3593e-8*(Frequency-2800)^2 **R^2: 0.472538**	SAC = 0.6062288 + 7.2922e-5*Frequency - 2.8925e-8*(Frequency-2800)^2 **R^2: 0.548718**	SAC = 0.318842 + 8.9636e-5*Frequency - 2.7777e-8*(Frequency-2800)^2 **R^2: 0.925405**
Lidinoid	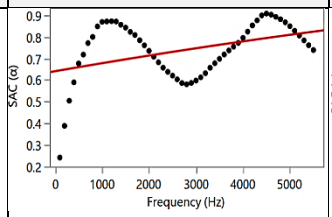	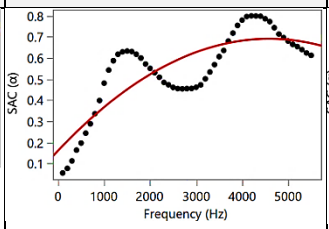	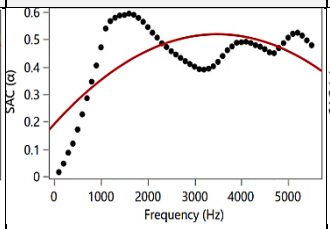	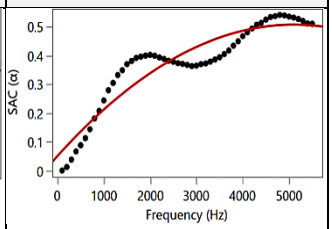
Polynomial Fit Degree=2	SAC = 0.6479233 + 3.3253e-5*Frequency - 8.596e-10*(Frequency-2800)^2 **R^2: 0.157354**	SAC = 0.3584855 + 8.9879e-5*Frequency - 2.515e-8*(Frequency-2800)^2 **R^2: 0.675683**	SAC = 0.4022568 + 3.7088e-5*Frequency - 2.699e-8*(Frequency-2800)^2 **R^2: 0.406559**	SAC = 0.1886164 + 8.0613e-5*Frequency - 1.7502e-8*(Frequency-2800)^2 **R^2: 0.876605**
Split P	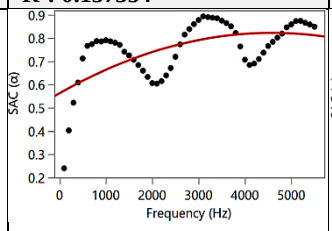	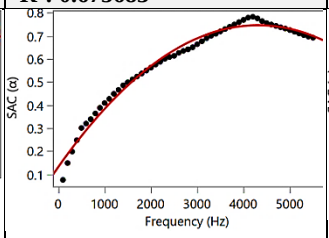	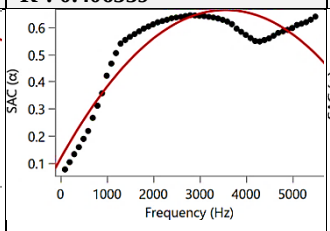	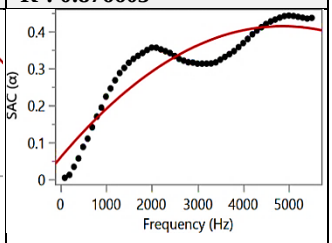
Polynomial Fit Degree=2	SAC = 0.6604508 + 4.4187e-5*Frequency - 1.24e-8*(Frequency-2800)^2 **R^2: 0.371303**	SAC = 0.3907799 + 9.968e-5*Frequency - 3.2945e-8*(Frequency-2800)^2 **R^2: 0.984383**	SAC = 0.4525862 + 6.6362e-5*Frequency - 4.3258e-8*(Frequency-2800)^2 **R^2: 0.843858**	SAC = 0.1775468 + 0.0000621*Frequency - 1.5081e-8*(Frequency-2800)^2 **R^2: 0.838118**

Figure 7 Experimental and curve fitting results of the TPMS lattices.

3.3. Effect of the surface type

According to a comparison of the data shown in **Figure 8**, four TPMS samples generated the greatest and lowest absorption coefficients under the four porosity conditions. At three lower porosity ranges, the gyroid and diamond structures clearly have larger absorption coefficients. The size of the unit cell is different for each lattice and has an impact on sound absorption. **Figure 8** displays the role of a small unit cell in getting a good sound absorption

value. In comparison to other TPMS lattices, the gyroid lattice has a smaller unit cell size (9.75) and produces superior results. The 90% porosity gyroid lattice (Uc-19.25) has a nearly identical absorption coefficient to the 80% lidinoid lattice (Uc-19). Gyroid has given better results at two porosity levels, and both absorption values are above 0.9, which is a good signal in terms of the efficient absorber. Gyroid demonstrates uniform results at initial, medium, and higher frequency ranges. Whereas diamond lattice has better sound absorption at low and high-frequency levels.

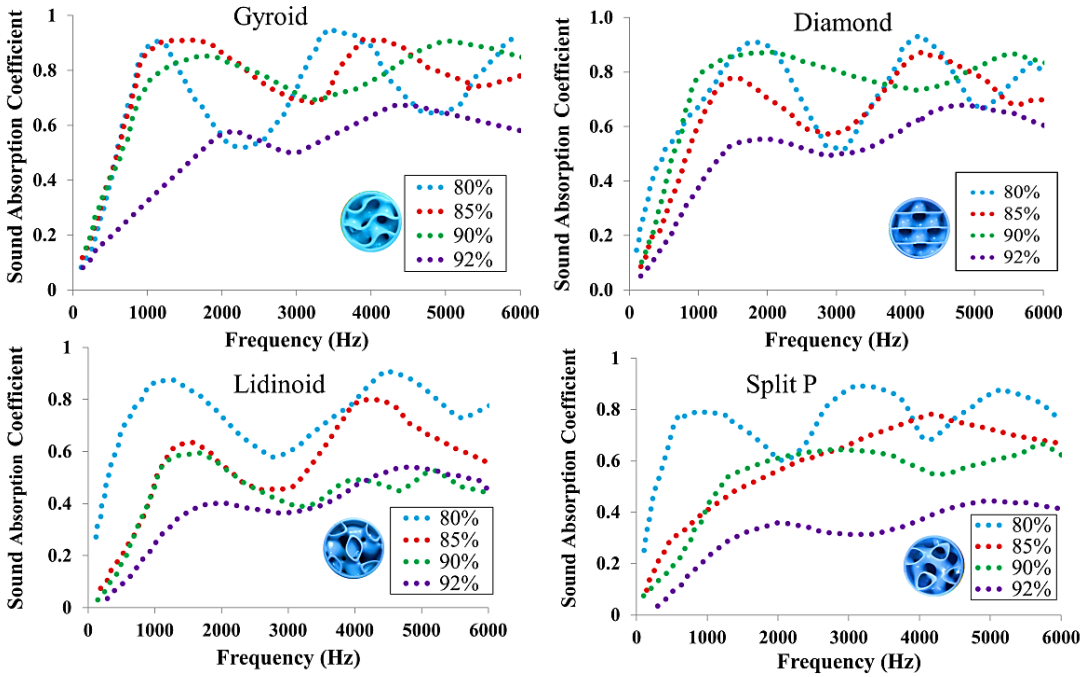

Figure 8 Effects of different TPMS surfaces on sound absorption characteristics.

3.4. Effect of the thickness/sample length

According to the above results, gyroid and diamond lattices have been selected for further processing to measure the effects of sample thickness on sound absorption characteristics. The 80% porosity and 32mm diameter parameters have been fixed for both lattices. Gyroid and diamond lattice structures were designed and additively developed with sample thicknesses of 55, 60, and 65mm. The sound absorption coefficient curves for both lattices with fixed porosity and various thicknesses are shown in **Figure 9**. A total of six designs have been made according to porosity and thickness.

From the data, it can be observed that both gyroid and diamond lattices with a small thickness of 55mm exhibited extremely poor acoustic absorption for lower frequencies (0.2, and 0.14), While at high frequencies, sound absorption values are acceptable. the highest sound absorption for diamond and gyroid lattices are 0.45 and 0.56 respectively.

The lattice thickness slightly improves sound absorption at higher excitation frequencies. The absorption coefficient improved less in gyroid lattice structures with constant porosity and variable sample thickness. The effective absorption frequency range for gyroid samples with a thickness of 65 mm is around 5000–6400 Hz. Two absorption peaks have been identified, the second of which has a higher value of 0.942. Compared to the 60 mm thickness, the 65 mm thickness gyroid curve shifted to the right, causing effective absorption frequency changes. Gyroids with a 60 mm thickness outperform in terms of total absorption performance for both lower and higher frequency ranges. The same phenomenon has been observed for the diamond lattice in **Figure 9**. While increasing the thickness of the diamond lattice, the peak frequency shifts to a higher frequency. The identical behaviour of the gyroid and diamond lattices has been noticed for 60mm and 65mm sample thicknesses. Nonetheless, enhancing the lattice thickness increases the price of additively manufactured resin models. Additionally, sample thickness should be kept to a minimum to make the structures for industrial applications smaller and lighter.

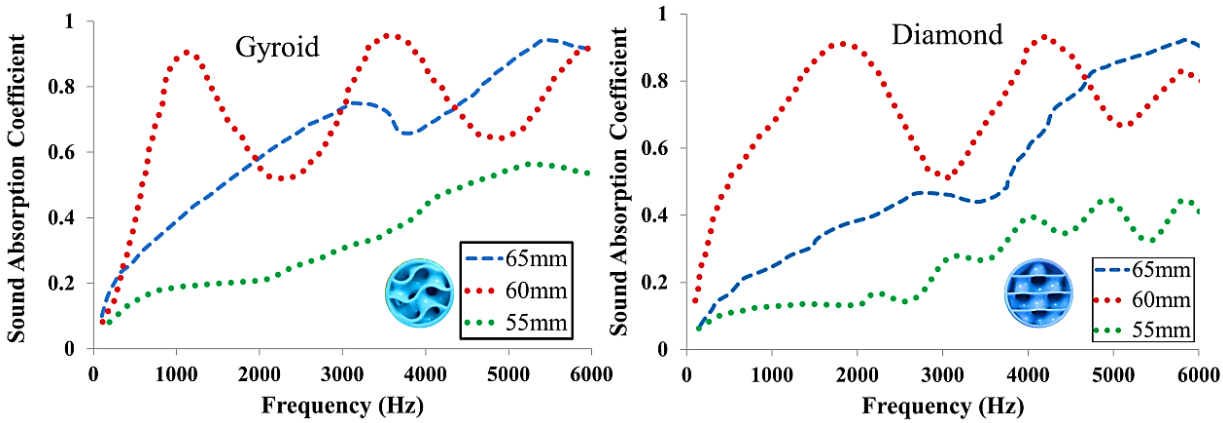

Figure 9 Effect of lattice thickness on sound absorption characteristics.

3.5. Effects of Wall Thickness

Wall thickness affects the surface area and porosity of the lattice, although the sound absorption behavior is not significantly affected. Wall thickness has little effect on the lattice's curve path, although thinner walls may marginally enhance the passage of sound waves during reflection and absorption. In addition, to reveal the impact of wall thickness on sound absorption, three gyroid lattice samples with different wall thicknesses (0.6-0.8-1mm) have been printed and tested. The results for each of the three wall thicknesses show a little variation in the absorption behavior, or less than 0.015.

3.6. NRC and Average SAC

The work compares the efficacy of sound absorption using the noise reduction coefficient (NRC) model across the four TPMS lattices. The arithmetic average of the NRC was determined for frequencies of 250, 500, 1000, and 2000 Hz octaves for the G, D, L, and SP lattices. The NRC of a sound-absorbing material must typically be larger than or equal to 0.20. The outcome demonstrates that lattices with less porosity have more significant noise reduction coefficient results. **Figure 10** illustrates the connection between the NRC and the porosity of TPMS structures. The gyroid lattice with 80% porosity showed higher values of the noise reduction coefficient (0.9) at frequencies between 1000 and 1100 Hz. Gyroid and diamond at medium porosity (85-90%) have averaged NRC values of 0.83 and 0.75, respectively. Conversely, the lowest values of the noise reduction coefficient were obtained from the lidinoid and split P (0.48 and 0.41). Higher-porosity lattices were ineffective at absorbing low-frequency sound but excelled in the high-frequency range. The NRC results for 85-90% porosity and a 60 mm thick gyroid lattice are higher than those of the 80% variant. In 92% porosity, all lattices show poor NRC performance. As a result, gyroid and diamond samples exhibited superior noise-dampening abilities compared to other structural kinds.

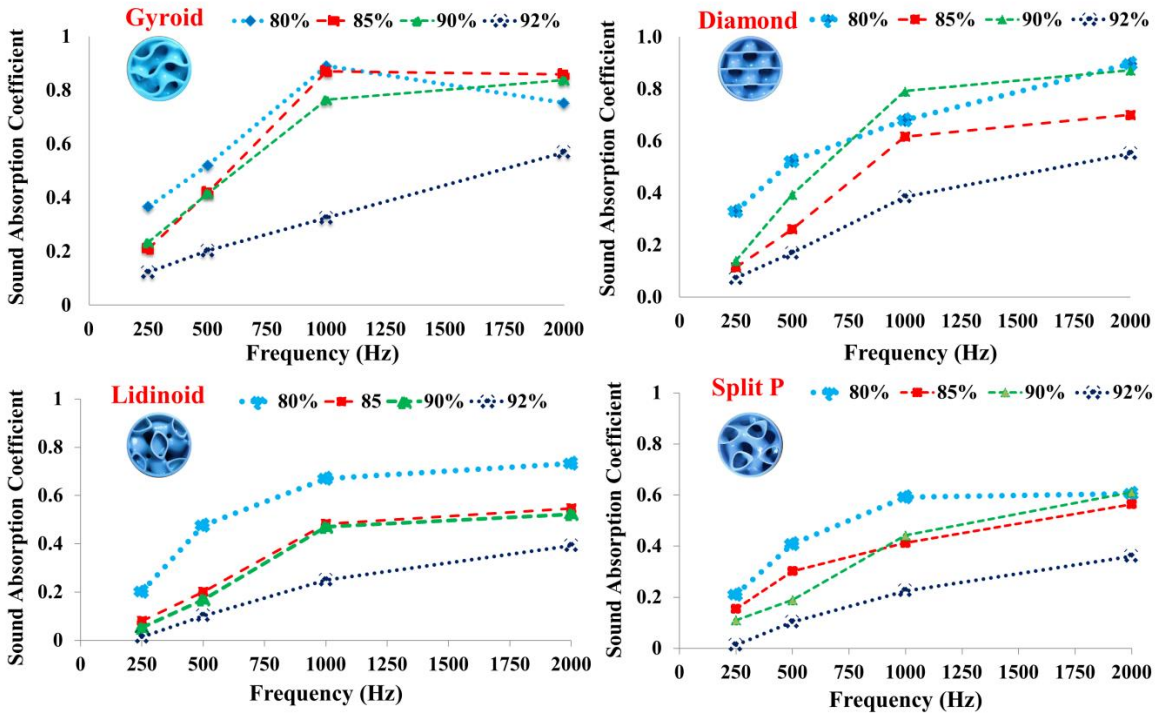

Figure 10 Noise reduction values for all TPMS structures.

Additionally, the impact of various thicknesses (55-60-65mm) on NRC values was noted for diamond and gyroid lattices with a constant 80% porosity. **Figure 11** clearly shows, however, that the NRC performance drops when the lattice thickness is either larger or smaller than 60 mm. Moreover, for lower to higher frequency ranges, the higher thickness lattices (65 mm) provide a progressive sound absorption pattern, while the 55 mm thickness lattice gives almost uniform sound absorption values at all frequencies.

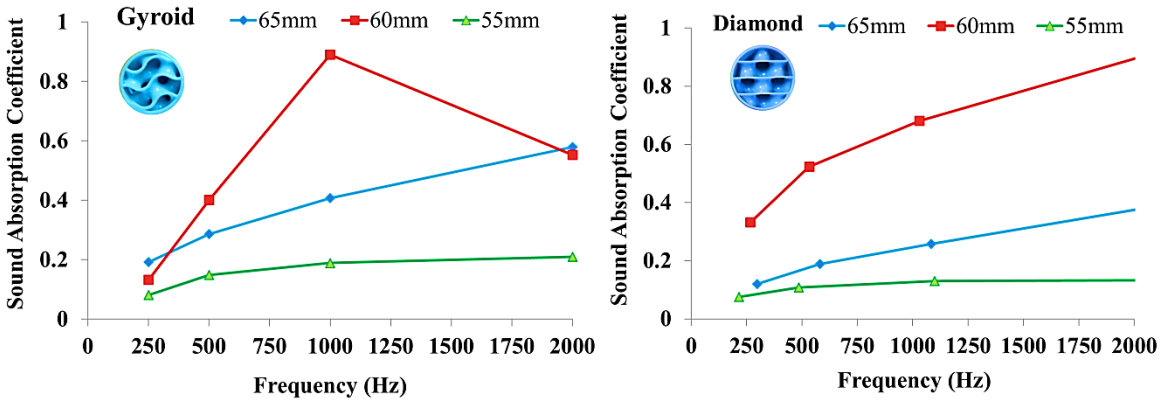

Figure 11 Noise reduction coefficient results for different lattice thicknesses.

4. Conclusion

Triply periodic minimal surface family lattices were taken into consideration as expected long-lasting and effective sound absorbers, Although fiber, composite, and volume-based lattice absorbers are extensively utilized in the area of acoustics. The work discussed the absorption performance of additively manufactured polymer samples, which were motivated by TPMS lattice structures (Gyroid, Diamond, Lidinoid, and Split P) that have been investigated. The tested lattices were also produced with different porosities, sample thicknesses, and wall thicknesses. Using experimental data obtained from a standard impedance tube, this article identifies TPMS lattices as effective sound absorbers. The influence of geometrical factors (surface, porosity, sample thickness, and wall thickness) of a TPMS lattice on sound absorption is presented in this paper. These are some of the significant findings of this study:

- In comparison to other structures, the resin-made gyroid lattice samples performed better in terms of sound absorption. This happened because the gyroid lattice had more complex pore geometries, which made it harder for air to flow through while sound waves were moving through the porous structure.
- The porosity of a lattice is one of the primary factors that influences its ability to absorb sound. Less dense and more open structures (92% porosity) show improved sound

absorption at high frequencies, whereas diamond and gyroid lattices in the 80–90% porosity range demonstrate higher absorption behavior at each frequency.

- The qualities of sound absorption are strongly influenced by lattice surface area and pore size. Sound absorption is increased by a larger surface area and a smaller pore size. Gyroid and diamond lattice samples with 80% porosity and a 60mm sample thickness have noise reduction coefficients and average sound absorption beyond the permitted range (above 0.5).
- The polynomial curve fitting results show that optimal SAC values have been identified throughout a wide frequency range, with the best curve fit for higher porosity structures such as Split P-0.984, Diamond-0.829, Gyroid-0.925, and Lidinoid-0.877.
- Gyroid and diamond lattices with extended thickness and low porosity exhibit progressive sound absorption behavior, which is excellent for the higher frequency range. A minor effect of lattice wall thickness on the acoustic property has been addressed.
- Lattices with more than 90% porosity with all thickness variants demonstrate poor NRC and average sound absorption.
- The thermal absorption impact of sound was not investigated in the current study. In these cases, ABS-like material proves to be more cost-effective than metal samples.

Potential future challenges may concern the printing of samples with a porosity below 75% for absorption testing and to understand the effects of dense and small void structures. In addition, variations in lattice diameter can be investigated, allowing us to observe how resonance effects within the lattice change. Furthermore, the combinations of two or three lattices may impact the acoustic performance.

Conflicts of Interest:

The authors declared no conflict of interest.

Acknowledgment

Not applicable.

Availability of data and materials

On request, the corresponding authors will provide all information and materials necessary to produce the findings in this study.

Funding

No funding is associated with this research.

Declarations

Ethical approval

The authors declare that there is no ethical issue applied to this article.

Abbreviations

The following abbreviations are used in this manuscript:

3D	*Three dimensional*
SLA	*Stereolithography*
TPMS	*Triply periodic minimal surface*
PLA	*Polylactic acid*
AM	*Additive Manufacturing*
PPI	*Pores per inch*
STL	*Standard triangle language*
CAD	*Computer-aided design*
φ	*porosity*
σ	*Flow resistivity*
NRC	*Noise reduction coefficient*
SAC	*Sound absorption coefficient*
Uc	*Unit cells*
Rs	*Specific flow resistance*

References

1. Zhao M, Li X, Zhang DZ, Zhai W (2023) TPMS-based interpenetrating lattice structures: Design, mechanical properties and multiscale optimization. Int J Mech Sci 244:108092. https://doi.org/10.1016/J.IJMECSCI.2022.108092
2. Baobaid N, Ali MI, Khan KA, Abu Al-Rub RK (2022) Fluid flow and heat transfer of porous TPMS architected heat sinks in free convection environment. Case Stud Therm Eng 33:101944. https://doi.org/10.1016/J.CSITE.2022.101944
3. Yang W, An J, Chua CK, Zhou K (2020) Acoustic absorptions of multifunctional polymeric cellular structures based on triply periodic minimal surfaces fabricated by stereolithography. Virtual Phys Prototyp 15:242–249. https://doi.org/10.1080/17452759.2020.1740747
4. Ho TYK, Ng AYR, Ye P, et al (2023) Realization of vat photopolymerisation of dense

SiC ceramics with SiO2/MgSO4 coated sub-micron powders for efficient heat dissipation. Addit Manuf 73:103664. https://doi.org/https://doi.org/10.1016/j.addma.2023.103664

5. Bankapalli NK, Gupta V, Saxena P, et al (2023) Filament fabrication and subsequent additive manufacturing, debinding, and sintering for extrusion-based metal additive manufacturing and their applications: A review. Compos Part B Eng 110915. https://doi.org/https://doi.org/10.1016/j.compositesb.2023.110915
6. Shah SWA, Xu Q, Ullah MW, et al (2023) Lignin-based additive materials: A review of current status, challenges, and future perspectives. Addit Manuf 74:103711. https://doi.org/https://doi.org/10.1016/j.addma.2023.103711
7. Chouhan G, Bala Murali G (2023) Designs, advancements, and applications of three-dimensional printed gyroid structures: A review. Proc Inst Mech Eng Part E J Process Mech Eng 0: https://doi.org/10.1177/09544089231160030
8. Babamiri BB, Barnes B, Soltani-Tehrani A, et al (2021) Designing additively manufactured lattice structures based on deformation mechanisms. Addit Manuf 46:102143. https://doi.org/10.1016/J.ADDMA.2021.102143
9. Benedetti M, Du Plessis A, Ritchie RO, et al (2021) Architected cellular materials: A review on their mechanical properties towards fatigue-tolerant design and fabrication. Mater Sci Eng R 144:100606. https://doi.org/10.1016/j.mser.2021.100606
10. Kladovasilakis N, Tsongas K, Kostavelis I, et al (2022) Effective Mechanical Properties of Additive Manufactured Strut-Lattice Structures: Experimental and Finite Element Study. Adv Eng Mater 24:2100879. https://doi.org/10.1002/ADEM.202100879
11. Großmann A, Gosmann J, Mittelstedt C (2019) Lightweight lattice structures in selective laser melting: Design, fabrication and mechanical properties. Mater Sci Eng A 766:138356. https://doi.org/10.1016/J.MSEA.2019.138356
12. Pelanconi M, Zavattoni S, Cornolti L, et al (2021) Application of Ceramic Lattice Structures to Design Compact, High Temperature Heat Exchangers: Material and Architecture Selection. Materials (Basel) 14:. https://doi.org/10.3390/MA14123225
13. Qin D, Sang L, Zhang Z, et al (2022) Compression Performance and Deformation Behavior of 3D-Printed PLA-Based Lattice Structures. Polymers (Basel) 14:1062. https://doi.org/10.3390/POLYM14051062
14. Giulio E Di, Auriemma F, Napolitano M, Dragonetti R (2021) Acoustic and thermoacoustic properties of an additive manufactured lattice structurea). J Acoust Soc

Am 149:3878. https://doi.org/10.1121/10.0005085

15. Chen Pan, Yafeng Han* and JL (2020) Design and Optimization of Lattice Structures : A Review. Appl sc 10:
16. Yu S, Sun J, Bai J (2019) Investigation of functionally graded TPMS structures fabricated by additive manufacturing. Mater Des 182:108021. https://doi.org/10.1016/J.MATDES.2019.108021
17. Chen H (2019) Minimal Twin Surfaces. Exp Math 28:404–419. https://doi.org/10.1080/10586458.2017.1413455
18. Roohani I (2023) Liquid Crystal Display Technique (Lcd) for High Resolution 3d Printing of Triply Periodic Minimal Surface Lattices Bioceramics. Addit Manuf 74:103720. https://doi.org/10.1016/j.addma.2023.103720
19. Zhou H, Zhao M, Ma Z, et al (2020) Sheet and network based functionally graded lattice structures manufactured by selective laser melting: Design, mechanical properties, and simulation. Int J Mech Sci 175:105480. https://doi.org/10.1016/J.IJMECSCI.2020.105480
20. Iyer J, Moore T, Nguyen D, et al (2022) Heat transfer and pressure drop characteristics of heat exchangers based on triply periodic minimal and periodic nodal surfaces. Appl Therm Eng 209:118192. https://doi.org/10.1016/J.APPLTHERMALENG.2022.118192
21. Al-Ketan O, Pelanconi M, Ortona A, Abu Al-Rub RK (2019) Additive manufacturing of architected catalytic ceramic substrates based on triply periodic minimal surfaces. J Am Ceram Soc 102:6176–6193. https://doi.org/10.1111/JACE.16474
22. Stan A, Milodin NL (2020) Robotic arm structural frame enhancement by gyroid lattice cube integration. Int J Mechatronics Appl Mech 2:7–13. https://doi.org/10.17683/ijomam/issue8.33
23. Thomas N, Sreedhar N, Al-Ketan O, et al (2018) 3D printed triply periodic minimal surfaces as spacers for enhanced heat and mass transfer in membrane distillation. Desalination 443:256–271. https://doi.org/10.1016/J.DESAL.2018.06.009
24. Elliott O, Gray S, McClay M, et al (2017) Design and Manufacturing of High Surface Area 3D-Printed Media for Moving Bed Bioreactors for Wastewater Treatment. J Contemp Water Res Educ 160:144–156. https://doi.org/10.1111/J.1936-704X.2017.03246.X
25. Lin C, Wen G, Yin H, et al (2022) Revealing the sound insulation capacities of TPMS sandwich panels. J Sound Vib 540:117303. https://doi.org/10.1016/j.jsv.2022.117303

26. Lu JY, Alzaabi F, Teneiji M Al, Lee DW (2021) Acoustic band structures of Architectured Materials based on Triply Periodic Minimal Surfaces. 15th Int Congr Artif Mater Nov Wave Phenomena, Metamaterials 1–3. https://doi.org/10.1109/Metamaterials52332.2021.9577144
27. Chua JW, Li X, Yu X, Zhai W (2023) Novel slow-sound lattice absorbers based on the sonic black hole. Compos Struct 304:116434. https://doi.org/10.1016/J.COMPSTRUCT.2022.116434
28. Vasina M, Monkova K, Monka PP, et al (2020) Study of the sound absorption properties of 3D-printed open-porous ABS material structures. Polymers (Basel) 12:1–14. https://doi.org/10.3390/POLYM12051062
29. Sun X, Jiang F, Wang J (2020) Acoustic Properties of 316L Stainless Steel Lattice Structures Fabricated via Selective Laser Melting. Metals (Basel) 10:111. https://doi.org/10.3390/MET10010111
30. Kimura M, Kunio J, Schuhmacher A, Ryu Y (2014) A new high-frequency impedance tube for measuring sound absorption coefficient and sound transmission loss. INTERNOISE 2014 - 43rd Int Congr Noise Control Eng Improv World Through Noise Control
31. Zhao Y, Xu J, Davy JL, et al (2022) Prediction of random incidence sound absorption coefficients of porous materials. Appl Acoust 189:108625. https://doi.org/10.1016/J.APACOUST.2021.108625
32. Niresh J, Neelakrishnan S, Subha Rani S (2016) Investigation and correction of error in impedance tube using intelligent techniques1. J Appl Res Technol JART 14:405–414. https://doi.org/10.1016/J.JART.2016.09.003
33. Gilbert R (2008) Chapter 10 - Noise. In: Gilbert RBT-AQG to H and S (ed). Woodhead Publishing, pp 83-90,https://doi.org/10.1016/B978-1-84569-499–9.5
34. Chen W, Hu S, Cao H, et al (2019) Review on Research process of Sound reduction Materials. IOP Conf Ser Mater Sci Eng 612:. https://doi.org/10.1088/1757-899X/612/5/052062
35. Liu Y, Lyu L, Guo J, Wang Y (2020) Sound absorption performance of the poplar seed Fiber/PCL composite materials. Materials (Basel) 13:. https://doi.org/10.3390/MA13061465
36. Pacheco MLM, Mejía FC, Lazcano YR, et al (2023) Determination of the Sound Absorption Capacity of Hydraulic Concrete Mixtures Added with Waste Tire Rubber. J Miner Mater Charact Eng 11:197–211. https://doi.org/10.4236/JMMCE.2023.115015

37. Günther F, Pilz S, Hirsch F, et al (2023) Shape optimization of additively manufactured lattices based on triply periodic minimal surfaces. Addit Manuf 73:103659. https://doi.org/10.1016/j.addma.2023.103659
38. Gao W, Zhang Y, Ramanujan D, et al (2015) The status, challenges, and future of additive manufacturing in engineering. Comput Des 69:65–89. https://doi.org/10.1016/J.CAD.2015.04.001
39. Li N, Huang S, Zhang G, et al (2019) Progress in additive manufacturing on new materials: A review. J Mater Sci Technol 35:242–269. https://doi.org/10.1016/J.JMST.2018.09.002
40. Chouhan G, Gunji B, Bidare P, et al (2023) Experimental and Numerical Investigation of 3D Printed Bio-inspired Lattice Structures for Mechanical Behaviour Under Quasi Static Loading Conditions. Mater Today Commun 105658. https://doi.org/10.1016/J.MTCOMM.2023.105658
41. Singh J, Chawla K, Singh R (2020) Applications of Thermoplastic Polymers in 3D Printing. Ref Modul Mater Sci Mater Eng. https://doi.org/10.1016/B978-0-12-820352-1.00010-9
42. Boparai KS (2020) Applications of Thermosetting Polymers in 3D Printing. Ref Modul Mater Sci Mater Eng 0: https://doi.org/10.1016/B978-0-12-820352-1.00036-5
43. Deshmukh S, Ronge H, Ramamoorthy S (2019) Design of periodic foam structures for acoustic applications: Concept, parametric study and experimental validation. Mater Des 175:107830. https://doi.org/10.1016/J.MATDES.2019.107830
44. Liu J, Chen T, Zhang Y, et al (2019) On sound insulation of pyramidal lattice sandwich structure. Compos Struct 208:385–394. https://doi.org/10.1016/j.compstruct.2018.10.013
45. Peng X, Ji J, Jing Y (2018) Composite honeycomb metasurface panel for broadband sound absorption. J Acoust Soc Am 144:EL255. https://doi.org/10.1121/1.5055847
46. An X, Lai C, Fan H, Zhang C (2020) 3D acoustic metamaterial-based mechanical metalattice structures for low-frequency and broadband vibration attenuation. Int J Solids Struct 191–192:293–306. https://doi.org/10.1016/J.IJSOLSTR.2020.01.020
47. Lan Y, Merkel T, Sarradj E (2023) Modified two-microphone method: Determination of acoustic properties in upper audible and lower ultrasonic range using impedance tube based on two MEMS microphones. Appl Acoust 211:109509. https://doi.org/https://doi.org/10.1016/j.apacoust.2023.109509
48. Chouhan G, Gunji B (2023) Additive manufacturing TPMS lattice structures:

Experimental study on airflow resistivity. Results Mater 100478. https://doi.org/10.1016/J.RINMA.2023.100478

49. Deaconu M, Toma AC, Dragasanu LI, Mihai D (2017) Comparative study of sound absorption coefficient determination using FEM method and experimental tests on Kundt's tube. AIP Conf Proc 1836:. https://doi.org/10.1063/1.4982001
50. Dixit T, Al-Hajri E, Paul MC, et al (2022) High performance, microarchitected, compact heat exchanger enabled by 3D printing. Appl Therm Eng 210:118339. https://doi.org/10.1016/J.APPLTHERMALENG.2022.118339
51. Singh Rathore S, Mehta B, Kumar P, Asfer M (2023) Flow Characterization in Triply-Periodic-Minimal-Surface (TPMS) based Porous Geometries: Part 1-Hydrodynamics. Transp Porous Media 146:669–701. https://doi.org/DOI: 10.1007/s11242-022-01880-7
52. Lehder EF, Ashcroft IA, Wildman RD, et al (2021) A multiscale optimisation method for bone growth scaffolds based on triply periodic minimal surfaces. Biomech Model Mechanobiol 20:2085–2096. https://doi.org/10.1007/S10237-021-01496-8/FIGURES/13
53. Karakoç A (2021) RegionTPMS — Region based triply periodic minimal surfaces (TPMS) for 3-D printed multiphase bone scaffolds with exact porosity values. SoftwareX 16:. https://doi.org/10.1016/J.SOFTX.2021.100835
54. Zhou L, Sigmund O, Zhang W (2021) Self-supporting structure design with feature-driven optimization approach for additive manufacturing. Comput Methods Appl Mech Eng 386:114110. https://doi.org/10.1016/J.CMA.2021.114110
55. Sankineni R, Ravi Kumar Y (2021) Evaluation of energy absorption capabilities and mechanical properties in FDM printed PLA TPMS structures. Proc Inst Mech Eng Part C J Mech Eng Sci 236:3558–3577. https://doi.org/10.1177/09544062211039530
56. Stansbury JW, Idacavage MJ (2016) 3D printing with polymers: Challenges among expanding options and opportunities. Dent Mater 32:54–64. https://doi.org/10.1016/J.DENTAL.2015.09.018
57. Ryan J, Dizon C, Catherine C, et al (2021) Post-Processing of 3D-Printed Polymers. Technologies 9:61. https://doi.org/10.3390/TECHNOLOGIES9030061